Journal of Molecular Structure 980 (2010) 24–30

Contents lists available at ScienceDirect

Journal of Molecular Structure

journal homepage: www.elsevier.com/locate/molstruc

Infrared and Raman spectra, vibrational assignment, NBO analysis and DFT calculations of 6-aminoflavone

Y. Erdogdu [a,*], O. Unsalan [b], M. Amalanathan [c], I. Hubert Joe [c]

[a] Department of Physics, Ahi Evran University, 40040 Kirsehir, Turkey
[b] Science Faculty, Department of Physics, Istanbul University, 34134 Istanbul, Turkey
[c] Centre for Molecular and Biophysics Research, Department of Physics, Mar Ivanios College, Thiruvananthapuram 695 015, Kerala, India

ARTICLE INFO

Article history:
Received 12 April 2010
Received in revised form 26 June 2010
Accepted 29 June 2010
Available online 6 July 2010

Keywords:
FT-infrared
FT-Raman
DFT
6-Aminoflavone
NBO

ABSTRACT

In this study, the experimental and theoretical study on the FT-infrared and FT-Raman spectra of 6-aminoflavone (6AF) are presented. The FT-IR (4000–400 cm^{-1}) and FT-Raman (3500–50 cm^{-1}) spectral measurements of solid sample of 6AF have been done. The geometric structure, conformational analysis, vibrational wavenumbers of 6AF in the ground state have been calculated by using Density Functional Method (B3LYP) with 6-311++G(d,p) as basis set. The normal modes were assigned by potential energy distribution (PED) calculations. A detailed vibrational spectral analysis was carried out and assignments of the observed bands have been proposed on the basis of fundamentals. Theoretically predicted vibrational wavenumbers were compared with available experimental data of molecule. The present experimental analysis on vibrational modes of 6AF can be well supported by theoretical analysis.

1. Introduction

The aminoflavone and its analogue (AF) exhibits anti-proliferative activity against several renal, breast, and ovarian cancer cell lines. They have showed the antitumor activity in vitro, particularly against neoplastic cells of renal origin. Pérez et al. identified cellular correlates of responsiveness to AF in continuous human tumor renal cell carcinoma lines and in tumor cell isolates, termed renal carcinoma cell strains, from patients with clear cell and papillary renal neoplasm's [1,2].

Almost all flavone derivatives have been identified from botanical sources, they are commonly found in vascular plants as phenyl-benzopyrones with different basic structures. Flavone and flavonols found in plants are yellow compounds and are the main components of a number of natural dyes used in textile dyeing since antiquity [3]. Extracted from plants, they are easily hydrolyzed from the glycosides to their parent flavonoids and can be applied to textiles as mordant dyes. Owing to their activities in photosensitization, energy transport and cellular metabolism, many flavone derivatives are ingredients for biochemical and pharmacological products used as human diet supplements [4–9].

Flavonoids are an active area of research as these plant compounds have antioxidative properties, show probably protective effects against chronic diseases [10], and bind to a broad range of enzymes [11–13]. Flavonoids have been investigated by X-ray crystallography [14], electron spin resonance [15], FT-IR and Raman spectra [16,17]. Quantum chemical studies of flavonoids at semi-empirical level as well as *ab initio* calculation at the Hartree–Fock level [18–22] have been reported. The FT-IR, FT-Raman and DFT result on some flavone derivatives (Flavone [23], 6-chloroflavone [24], 6,8-dichloroflavone and 6,8-dibromoflavone [25] and Baicalein and Naringenin [26]) have been reported. In the present work, we report the results of theoretical and experimental (IR and Raman) spectra, conformational analysis and molecular orbital energies of 6AF molecule. The spectroscopic properties of 6AF have not yet been studied in detail to the best of our knowledge. Therefore, the present investigation was undertaken to study the vibrational spectra of 6AF molecule completely and to identify the various modes with greater wave number accuracy. Density Functional Theory (DFT/B3LYP) calculations have been performed to support molecular structure, hydrogen bonding harmonic force field, vibrational wavenumbers and IR and Raman intensities of the molecule. Furthermore, the present work interpreted the calculated spectra of 6-aminoflavone (6AF) in terms of total energy distributions (TED's) and made the assignment of the experimental bands due to TED analysis results. The natural bond orbital (NBO) analysis has been performed to elucidate the correlation between the intramolecular charge transfers (ICT), π-electron delocalization and intramolecular hydrogen bonding.

* Corresponding author. Tel.: +90 3862114557; fax: +90 3862114525.
E-mail address: yusuferdogdu@gmail.com (Y. Erdogdu).

0022-2860/$ - see front matter © 2010 Elsevier B.V. All rights reserved.
doi:10.1016/j.molstruc.2010.06.032

2. Experimental

The 6AF sample was purchased from Sigma–Aldrich Chemical Company with a stated purity of greater than 98% and it was used as such without further purification. The sample of 6AF is in powder form at room temperature. The infrared spectrum of the sample was recorded between 4000 cm^{-1} and 400 cm^{-1} on a Mattson 1000 FT-IR spectrometer which was calibrated using polystyrene bands. The sample was prepared as a KBr disc. The FT-Raman spectrum of the sample was recorded between 3500 and 50 cm^{-1} regions on a Bruker FRA 106/S FT-Raman instrument using 1064 nm excitation from an Nd:YAG laser. The detector is a liquid nitrogen cooled Ge detector.

3. Computational details

Density functional theoretical (DFT) computations of 6AF were performed by using Gaussian 03 program package [27] at the Becke–Lee–Yang–Parr hybrid exchange–correlation three-parameter functional (B3LYP) level with standard 6-31++G (d,P) basis set to derive the complete geometry optimization. All the optimized geometry corresponding to minimum on the potential energy surface has been obtained by solving self-consistent field equation iteratively. The calculated harmonic vibrational wavenumbers have been analytically calculated by taking second order derivative of energy using the similar level of theory. The calculated wavenumbers were scaled with scaling factors. The vibrational modes were assigned on the basis of PED analysis using VEDA 4 program [28].

The Raman activities (S_i) calculated with Gaussian 03 program converted to relative Raman intensities (I_i) using the following relationship derived from the intensity theory of Raman scattering.

$$I_i = \frac{f(\upsilon_0 - \upsilon_i)^4 S_i}{\upsilon_i[1 - \exp(hc\upsilon_i/kT)]} \quad (1)$$

where υ_0 is the exciting frequency in cm^{-1}, υ_i the vibrational wavenumber of the ith normal mode, h, c and k fundamental constants, and f is a suitably chosen common normalization factor for all peak intensities.

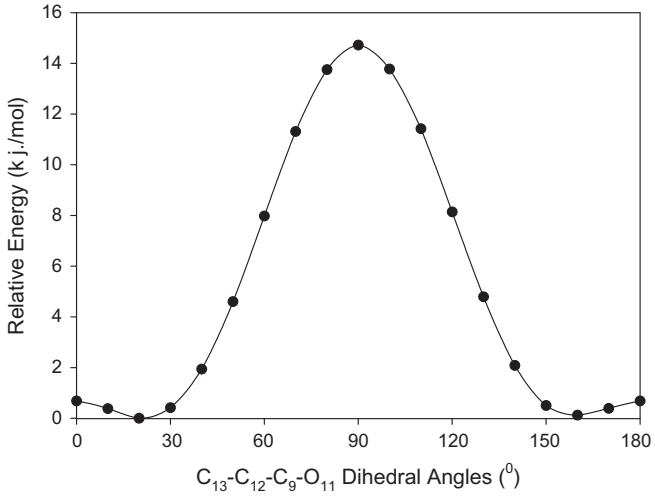

Fig. 1. Dihedral angle–relative energy curves of 6AF by B3LYP/6-311++G(d,p) level of theory.

4. Results and discussion

4.1. Conformational stability

In order to reveal all possible conformations of 6AF, a detailed potential energy surface (PES) scan in C_{13}–C_{12}–C_9–O_{11} dihedral angles was performed. The scan was carried out by minimizing the potential energy in all geometrical parameters by changing the torsion angle every 10° for 180° rotation around the bond. The shape of the potential energy as a function of the dihedral angle is illustrated in Fig. 1. Some flavone derivative [23–26] and 6AF molecules exhibit similar trends for conformational analysis.

4.2. Optimized geometry

The optimized molecular structure of 6AF (Fig. 2) was calculated using Gaussian 03 program. The optimized geometrical parameters are given in Table 1. Flavone consists of benzenic and pyranone rings in the same plane and the phenyl substituent out of this plane. The molecular structure is non-planar; the tilting takes place between the flavones ring and the phenyl ring around 20° is due to steric repulsion between the two rings. The dihedral angle (C_8–C_9–C_{12}–C_{14}) between the two planar rings and the phenyl group is 21.4°. Also the C–C inter-ring bond connecting

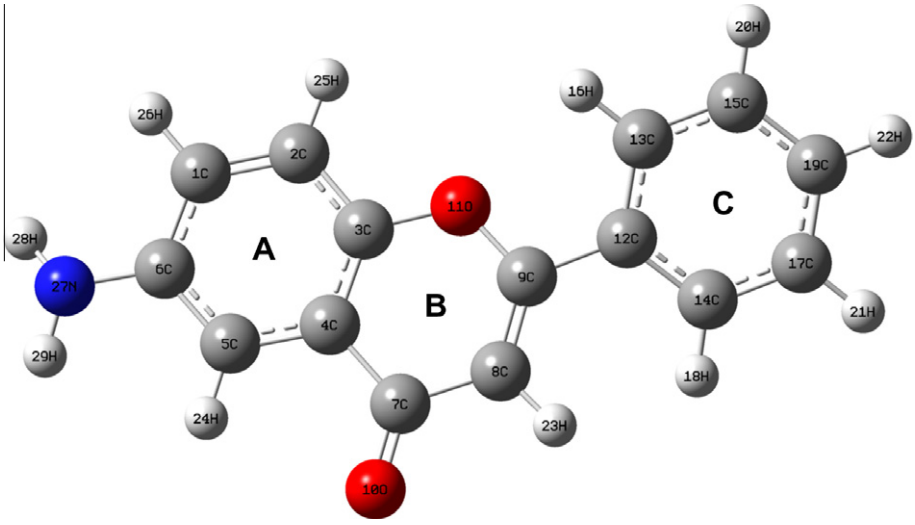

Fig. 2. Optimized molecular structure and atomic numbering of 6AF.

Table 1
The DFT level calculated optimized geometrical parameters.

Bond lengths	Value (Å)	Bond angles	Value (°)	Dihedral angles	Value (°)
C_1–C_2	1.383	C_1–C_2–C_3	119.4	C_1–C_2–C_3–C_4	0.32
C_2–C_3	1.396	C_2–C_3–C_4	120.7	C_2–C_3–C_4–C_5	−0.20
C_3–C_4	1.397	C_3–C_4–C_5	119.2	C_3–C_4–C_5–C_6	0.05
C_4–C_5	1.399	C_4–C_5–C_6	121.0	C_2–C_3–C_4–C_7	179.71
C_5–C_6	1.393	C_3–C_4–C_7	119.4	C_3–C_4–C_7–C_8	0.6
C_4–C_7	1.482	C_4–C_7–C_8	113.9	C_4–C_7–C_8–C_9	−1.20
C_7–C_8	1.453	C_7–C_8–C_9	122.7	C_3–C_4–C_7–O_{10}	−179.80
C_8–C_9	1.358	C_4–C_7–O_{10}	122.7	C_7–C_8–C_9–O_{11}	179.86
C_7–O_{10}	1.228	C_8–C_9–O_{11}	121.9	C_7–C_8–C_9–C_{12}	180.01
C_9–O_{11}	1.357	C_8–C_9–C_{12}	125.7	C_8–C_9–C_{12}–C_{13}	−158.29
C_9–C_{12}	1.476	C_9–C_{12}–C_{13}	120.4	C_8–C_9–C_{12}–C_{14}	21.44
C_{12}–C_{13}	1.403	C_9–C_{12}–C_{14}	120.8	C_9–C_{12}–C_{13}–C_{15}	178.90
C_{12}–C_{14}	1.403	C_{12}–C_{13}–C_{15}	120.5	C_9–C_{12}–C_{13}–H_{16}	−0.59
C_{13}–C_{15}	1.392	C_{12}–C_{14}–C_{17}	120.6	C_9–C_{12}–C_{14}–C_{17}	−179.00
C_{14}–C_{17}	1.082	C_{12}–C_{13}–H_{18}	120.0	C_9–C_{12}–C_{13}–H_{18}	2.23
C_{15}–C_{19}	1.394	C_{13}–C_{17}–C_{19}	120.3	C_{12}–C_{14}–C_{17}–C_{19}	−0.20
C_{13}–H_{16}	1.082	C_{13}–C_{15}–H_{20}	119.6	C_{12}–C_{13}–C_{15}–H_{20}	−179.53
C_{14}–H_{18}	1.083	C_{12}–C_{14}–H_{21}	120.6	C_{12}–C_{14}–C_{17}–H_{21}	−179.67
C_{15}–H_{20}	1.084	C_{17}–C_{19}–H_{22}	120.2	C_{14}–C_{17}–C_{19}–H_{22}	−179.95
C_{17}–H_{21}	1.084	C_7–C_8–H_{23}	117.2	C_4–C_7–C_8–H_{23}	177.7
C_{19}–H_{22}	1.084	C_4–C_5–H_{24}	117.5	C_3–C_4–C_5–H_{24}	−179.79
C_8–H_{23}	1.081	C_6–C_1–H_{25}	121.1	C_6–C_1–C_2–H_{25}	179.74
C_5–H_{24}	1.085	C_6–C_1–H_{26}	119.4	C_1–C_2–C_3–H_{26}	179.42
C_2–H_{25}	1.083	C_1–C_6–N_{27}	120.1	C_4–C_5–C_6–N_{27}	−177.11
C_1–H_{26}	1.085	C_6–N_{27}–H_{28}	116.1	C_5–C_6–N_{27}–H_{28}	−155.92
C_6–N_{27}	1.396	C_6–N_{27}–H_{29}	115.7	C_5–C_6–N_{27}–H_{29}	−20.89
C_{22}–H_{27}	1.009			C_9–C_{12}–C_{13}–H_{16}	−0.60
C_{23}–H_{28}	1.009				

the substituent to the pyranone ring shows a much higher double bond character, where C_4–C_7, C_7–C_8, C_9–C_{12} bonds are around 1.45 Å, the rest of the bond lengths in 6AF range from 1.37 to 1.40 Å. This may suggest that 6AF is a π electron delocalized system, a highly conjugated molecule, and hence shows small deviation from co-planarity. It seems that the oxygen O_{10} contributes to the delocalization of the π electrons in the system allowing the compound to behave aromatically. However, the C_4–C_7 and C_7–C_8 bond lengths of 1.48 Å and 1.45 Å, respectively, the pyranone ring must be slightly conjugated compared to the rest of the molecule. Furthermore, the C_9–C_{12} bond length of 1.47 Å is closer to that of a single bond than of a delocalized one, which suggests that the conjugation across the phenyl ring. Another important thing to notice is that C_8–C_9 [1.35 Å] and C_7–O_{10} [1.22 Å] bond lengths are smaller compared to the other bonds. This would suggest that the π electrons tend to be mostly localized in the vicinity of the C_8–C_9 and C_7–O_{10} bonds. From the above observations, one can confirm that the 6AF molecule is highly conjugated and π electron delocalized.

4.3. NBO analysis

The natural bond orbital (NBO) analysis provides a description of the structure of a conformer by a set of localized bond, antibonds and Rydberg extravalence orbitals. Stabilizing interactions between filled and unoccupied orbitals and destabilizing interactions between filled orbitals can also be obtained from this analysis [29–32]. Therefore, NBO theory is a valuable complement to the energetic and structural data presented above. DFT level computation is used to investigate the various second order interaction between the filled orbitals of one subsystem and vacant orbitals of another subsystem, which is a measure of the delocalization or hyperconjugation [33]. The main natural orbital interactions were analyzed with the NBO 5.0 program [34]. The hyperconjugative interaction energy was deduced from the second-order perturbation approach as:

$$E(2) = -n_\sigma \frac{\langle \sigma|F|\sigma\rangle^2}{\varepsilon_{\sigma^*} - \varepsilon_\sigma} = -n_\sigma \frac{F_{ij}^2}{\Delta E} \quad (2)$$

where $\langle \sigma|F|\sigma\rangle^2$, or F_{ij}^2 is the Fock matrix element between i and j NBO orbitals, ε_σ and ε_{σ^*} are the energies of σ and σ* NBO's, and n_σ is the population of the donor σ orbital.

The NBO analysis is an efficient method for investigating charge transfer (CT) or hyperconjugative interaction in molecular systems. Some electron donor orbital, acceptor orbital and the interacting stabilization energies resulting from the second-order micro disturbance theory have been reported [35]. The larger the $E(2)$ values, the more intensive is the interaction between electron donors and electron acceptors. The second-order perturbation theory analysis of Fock matrix in the NBO basis of the molecule shows strong intramolecular hyperconjugative interactions, which are presented Table 2. The most important interaction (n–σ*) energies, related to the resonance in the molecules, are electron donation from the LP(1)N atoms of the electron donating groups to the anti-bonding acceptor π*(C–C) of the phenyl ring (LP1N27 → σ*(C_1–C_6)) = 113.6 kJ/mol. This larger energy shows the hyperconjugation between the electron donating nitrogen and the phenyl ring. The intramolecular hyperconjugative interactions are formed by the orbital overlap between π(C–C) and π*(C–C) bond orbitals, which results in ICT (Intra molecular charge transfer) causing stabilization of the system. These interaction are observed as an increase in ED in C–C anti-bonding orbital that weakens their

Table 2
Second-order perturbation theory analysis of Fock matrix in NBO basis.

Donor(i)	ED(i) (e)	Acceptor(j)	ED(j) (e)	$E(2)$[a] (kJ mol^{-1})	$E(i)$–$E(j)$[b] (a.u.)	$F(I,j)$[c] (a.u.)	
π(C_1–C_6)	0.7022	π*(C_2–C_3)	0.7119	99.6	0.27	0.29	0.072
		π*(C_4–C_5)	0.7047	81.9			0.067
π(C_2–C_3)	0.7023	π*(C_1–C_6)	0.6887	79.7	0.29	0.30	0.067
		π*(C_4–C_5)	0.7047	86.8			0.071
π(C_4–C_5)	0.7095	π*(C_1–C_6)	0.6887	92.9	0.27	0.26	0.070
		π*(C_2–C_3)	0.7119	87.4	0.28		0.068
		π*(C_7–O_{10})	0.8228	81.8			0.067
π(C_{12}–C_{13})	0.7220	π*(C_8–C_9)	0.6762	63.2	0.28	0.28	0.060
		π*(C_{14}–C_{17})	0.7100	83.1	0.28		0.068
		π*(C_{15}–C_{19})	0.7040	81.5			0.067
π(C_{14}–C_{17})	0.7092	π*(C_{12}–C_{13})	0.6919	80.7	0.28	0.28	0.067
		π*(C_{15}–C_{19})	0.7040	84.9			0.068
π(C_{15}–C_{19})	0.7102	π*(C_{12}–C_{13})	0.6919	89.3	0.28	0.28	0.069
		π*(C_{14}–C_{17})	0.7100	81.5			0.067
LP1O10		σ*(C_4–C_7)	0.6856	9.6	1.13	1.16	0.046
	–	σ*(C_7–C_8)	0.7185	9			0.045
LP2O10	–	σ*(C_4–C_7)	0.6856	84.978.3	0.70	0.72	0.107
		σ*(C_7–C_8)	0.7185				0.105
LP1O11	–	σ*(C_2–C_3)	0.7114	3.2	1.11	1.11	0.026
		σ*(C_3–C_4)	0.7104	27.4	1.16	1.01	0.076
		σ*(C_8–C_9)	0.7124	24.9			0.075
		σ*(C_9–C_{12})	0.7094	4.4			0.029
LP2O11	–	σ*(C_2–C_3)	0.7114	99.8	0.36	0.37	0.087
		σ*(C_8–C_9)	0.7124	137.9			0.099
LP1N27	–	σ*(C_1–C_6)	0.6887	113.6	0.31		0.088

ED – electron density.
[a] $E(2)$ means energy of hyperconjugative interactions; cf. Eq. (2).
[b] Energy difference between donor and acceptor i and j NBO orbitals.
[c] $F(i,j)$ is the Fock matrix element between i and j NBO orbitals.

respective bonds [36]. The ED at the four conjugated π and π* bonds (~0.7 e) of the phenyl ring clearly demonstrate strong delocalization of electron leading to stabilization of (~80–90 kJ/mol). A very strong interaction has been observed between the π type orbital containing the lone electron pair of O_{11} and the neighbor $\sigma^*(C_2–C_3)$ $\sigma^*(C_8–C_9)$ anti-bonding orbital of the benzene ring. This interaction is responsible for a pronounced decrease of the lone pair orbital occupancy than the other occupancy, and is possible to hyperconjugation between O_{11} and the benzene ring. These ICT results support the bio activity of the molecule. The Mulliken population analysis in the flavone and 6-aminoflavone molecules was calculated using the B3LYP/6-311++G(d,p) level. The charge distributions structure and chart of flavone and 6-aminoflavone are shown in Fig. 3.

4.4. Vibrational analysis

The spectroscopic properties of 6AF have not yet been studied in detail to the best of our knowledge. The 6AF consists of 29 atoms, which has 81 vibrational degrees of freedom. The 81 normal modes of 6AF have been assigned according to the detailed vibrations of the individual atoms. These molecules belong to C_1 symmetry group. Scale factors were used to fit the calculated wave numbers with those of the observed ones [24,37,38]. Figs. 4 and 5 present the FT-Raman and FT-IR spectra of 6AF, respectively. The experimental FT-IR and FT-Raman wave numbers are tabulated in Table 3, together with the calculated wave numbers. As seen in tables IR absorption intensities of 6AF are in consistency with the PED results.

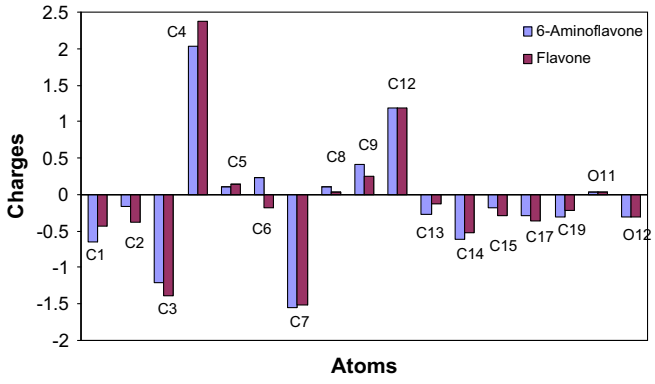

Fig. 3. The charge distributions structure of flavone and 6-aminoflavone.

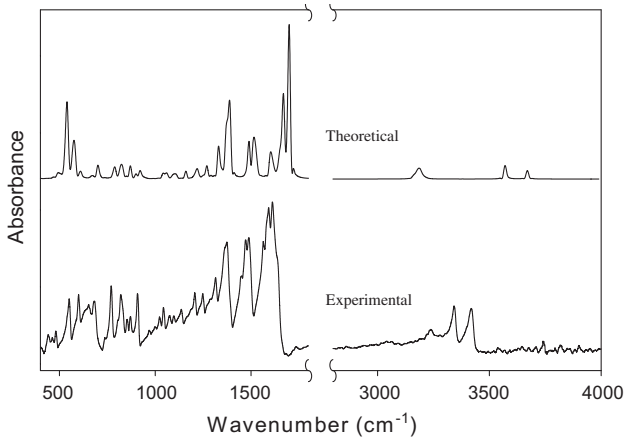

Fig. 4. Comparison of experimental and theoretical (B3LYP/6-311++G(d,p) FT-IR spectrum for 6AF.

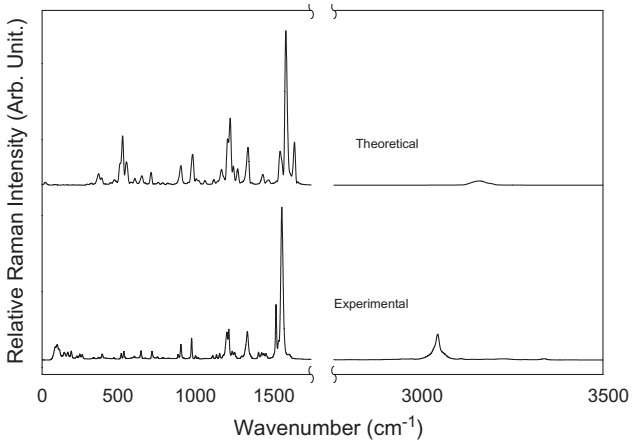

Fig. 5. Comparison of experimental and theoretical (B3LYP/6-311++G(d,p) FT-Raman spectrum for 6AF.

Aromatic amines absorb at slightly higher than aliphatic amines. These bands are shifted to higher wavenumbers due to hydrogen bonding. Generally, H-bonding leads to a reduction in NH_2 stretching wavenumbers, and increase in NH_2 bending wavenumber, a broadening of the spectral band and increase in IR intensity [38]. The asymmetric stretching vibration of aromatic primary amines was observed around 3500 cm^{-1} while the symmetric one around 3400 cm^{-1} [39]. The observed band in IR at 3422 cm^{-1} is assigned for the asymmetric N–H stretching mode. The symmetric N–H stretching mode was observed at 3344 cm^{-1} in IR and at 3347 cm^{-1} in Raman. The shifting to lower wavenumber of the N–H stretching mode could be interpreted as N–H intermolecular interaction [40]. The NH_2 in plane bending vibrations are observed in IR at 1076 cm^{-1}. The out of plane NH_2 vibrations appears from 850 to 700 cm^{-1}. The band observed at 872 cm^{-1} in FT-IR spectra is assigned the out of plane vibration of NH_2. The above assignments were seen to be in good agreement with those of the calculated data.

Normal esters are characterized by the strong IR absorptions due to the C=O stretching vibration in the range 1750–1735 cm^{-1} and the other due to C–O stretching vibration near 1200 cm^{-1}. The conjugated ester part gives intense IR band at 1720 cm^{-1} [41]. The increase in single bond character due to conjugation lowers the wavenumber of carbonyl and double bond absorptions. The carbonyl stretching vibration observed as an intense band at 1603 cm^{-1} in IR. The observed wavenumber of the carbonyl stretching vibration is lower due to the π-electron being localized. The bands duo to the ester C–O stretching vibration are strong, partly due to an interaction of C–C vibration and occur in the range 1300–1100 cm^{-1}. The observed bands in IR at 1375 cm^{-1} and Raman at 1374 cm^{-1} were assigned for C–O stretching vibration.

The bands occurs in the region 3080–3010 cm^{-1} and are strong to medium intensity is due to the aromatic C–H stretching wavenumbers. The intense band in Raman at 3127 cm^{-1} and 3069 cm^{-1} is assigned for C–H stretching wavenumber. The C–H in plane vibrations are appear in the region 1000–1290 cm^{-1}. The C–H in plane deformation is observed in Raman only 1271 cm^{-1} 1165 cm^{-1} The C–H out of plane vibration of the mono substituted ring is observed in the region 770–730 cm^{-1} and for the tri substituted ring is 800–760 cm^{-1}. In 6AF the C–H out of plane vibration are observed in IR at 854 cm^{-1} [ring B] and 822 cm^{-1} [ring C]. The intense band observed in IR and Raman at 770 cm^{-1} is due to C–H out of plane vibration of ring C. The observed band at 737 cm^{-1} in IR and 734 cm^{-1} in Raman is also due to C–H out of plane vibration of ring B.

Table 3
Vibrational wavenumbers of 6AF for B3LYP/6-311++G(d.p).

Unscaled frequency[a]	Scaled frequency[b]	I_{IR}[c]	I_{Raman}[d]	Exp. IR	Exp. Raman	TED[e] (%)
34	33	0.146	0.119	–	–	Γ_{OCCC}(89) B
47	45	0.225	0.103	–	–	Γ_{CCCC}(14) A + Γ_{COCC}(39)+γ_{CCCC}(16) B
95	91	0.110	0.110	–	87	δ_{OCC}(37) δ_{CCC}(16) γ_{CCCC}(13) B
111	107	0.577	0.078	–	114	Γ_{CCCC}(12) A Γ_{CCCC}(40) B
152	147	0.141	0.713	–	147	Γ_{CCOC}(57) B
177	171	0.329	0.294	–	170	Γ_{CCCC}(15) A Γ_{CCCC}(25) B Γ_{COCC}(17) B
218	210	0.696	0.443	–	193	δ_{CCO}(10) B Γ_{CCCC}(11) A Γ_{CCCC}(12) C
240	232	0.858	0.505	–	232	δ_{CCO}(18) B δ_{NCC}(12) A
260	251	0.140	0.018	–	251	υ_{CC}(24) (B–C) δ_{CCO}(11) B δ_{CCC}15 C
298	288	4.603	0.490	–	–	Γ_{HNCC}(95) A
337	326	1.279	1.150	–	344	δ_{OCC}(17) B δ_{CCC}(22) (B–C)
378	366	1.317	2.458	–	377	Γ_{CCCC}(20) γ_{NCCC}(11) A γ_{CCOC}(23) B
393	380	0.226	0.209	–	–	δ_{CCC}(10) A δ_{OCC}(43) B
410	397	0.019	0.024	–	–	Γ_{HCCC}(26) Γ_{CCCC}(65) C
435	420	0.152	6.624	–	402	Γ_{HCCC}(11) Γ_{CCCC}(52)A
469	454	0.517	40.22	441	–	γ_{CCCC}(14) (B–C)
494	478	3.867	18.23	481	481	δ_{CCC}(13) B δ_{CCC}(10) γ_{CCCC}(12) B–C
533	515	10.58	13.01	–	–	δ_{NCC}(11) A δ_{COC}(19) B
537	520	41.64	0.554	–	529	Γ_{HNCC}(26) γ_{NCCC}(11) A γ_{CCOC}(10) B
549	531	4.369	0.328	550	546	δ_{CCO}(15) B δ_{CCC}(11) A
575	556	31.85	1.411	–	–	Γ_{HNCC}(29) γ_{NCCC}(20) A γ_{CCOC}(10) B
612	592	3.576	0.066	–	–	δ_{OCC}(44) B δ_{CCC}(10) A
633	612	0.071	0.219	599	616	δ_{CCC}(65) C
667	645	1.527	0.359	–	–	Γ_{CCCC}(17) C + γ_{CCOC}(43)B
677	655	0.619	2.736	653	662	δ_{CCC}(25) C
695	673	1.208	0.669	–	–	Γ_{CCCC}(22) γ_{OCCC}(12) γ_{NCCC}(24) B
703	680	8.396	6.785	681	–	Γ_{HCCC}(37) Γ_{CCCC}(30) C
738	714	0.284	0.398	–	–	υ_{CC}(12) δ_{CCC}(11) δ_{CCC}(10) A
763	738	0.153	0.071	737	735	Γ_{HCCC}(12) γ_{OCCC}(34) γ_{CCOC}(15) B
786	760	8.900	3.157	770	770	Γ_{HCCC}(37) Γ_{CCCC}(32) γ_{CCOC}(10)C
816	789	4.938	6.430	–	–	υ_{OC}(20) δ_{CCC}(10) B
826	799	8.615	2.396	806	807	Γ_{HCCN}(46) Γ_{HCCC}(38) A
853	825	0.798	8.636	822	–	Γ_{HCCC}(91) C
870	842	6.355	0.352	854	–	Γ_{HCCC}(70) γ_{OCCC}(13) B
902	872	2.441	3.301	872	–	Γ_{HCCN}(62) Γ_{CCCC}(19) A
923	893	5.421	3.518	–	–	υ_{OC}(11) δ_{CCO}(12) B
936	905	0.568	0.280	909	911	δ_{CCC}(25) A Γ_{HCCC}(11) C
943	912	0.216	1.407	–	930	Γ_{HCCC}(56) C
953	921	0.282	0.183	–	–	Γ_{HCCN}(38) Γ_{HCCC}(45) A
990	957	0.102	0.067	970	–	Γ_{HCCC}(91) C
1006	973	0.026	0.026	–	–	Γ_{HCCC}(72) Γ_{CCCC}(11) C
1016	982	0.232	0.188	998	1000	υ_{CC}(11) δ_{CCC}(64) C
1044	1010	4.679	3.580	1023	1027	υ_{CC}(34) C υ_{OC}(13) B
1062	1027	2.894	1.283	1043	1146	υ_{OC}(19)
1094	1058	2.272	1.002	–	–	δ_{CCC}(37) A δ_{HCC}(13)
1101	1065	0.988	0.184	1076	–	υ_{CC}(19) δ_{HNC}(53) A
1108	1071	2.189	4.292	–	–	υ_{CC}(30) δ_{HCC}(39) C
1159	1121	3.859	10.120	–	–	υ_{CC}(17) δ_{HCC}(58) A
1185	1146	0.024	0.016	–	1165	δ_{HCC}(80) C
1207	1167	3.383	19.70	–	1187	δ_{HCC}(72) C
1222	1182	5.435	1.919	1207	–	υ_{C7C8}(11) υ_{OC}(28) B + δ_{HCC}(11) A
1254	1212	1.361	0.616	–	1237	υ_{CC}(19) δ_{HCC}(15) B
1268	1226	7.165	3.370	1248	1248	δ_{HCC}(40) B
1288	1246	0.967	3.913	–	1271	υ_{CC}(13) υ_{NC}(11) δ_{HCC}(13) A4 υ_{CC}(11) B
1318	1274	0.627	19.00	–	1287	υ_{CC}(18) C + υ_{NC}(10)A
1333	1289	20.62	2.607	–	–	υ_{CC}(11) C + υ_{NC}(10) + δ_{HCC}(10) A
1356	1311	2.321	2.232	1316	1333	υ_{CC}(22) + δ_{HCC}(59) C
1373	1328	26.87	33.73	–	–	υ_{CC}(45) A
1386	1341	57.18	45.03	1375	1374	υ_{CC}(10) + υ_{OC}(20) B
1477	1429	2.226	4.592	1449	1447	δ_{HCC}(48) C
1488	1439	19.82	25.87	1472	1468	υ_{CC}(14) A
1515	1465	29.01	3.112	1489	1484	δ_{HCC}(30) + δ_{CCC}(11) A
1526	1476	13.18	1.651	–	1497	δ_{HCC}(56) C
1604	1551	21.04	0.573	1564	1565	υ_{CC}(33) A
1618	1564	3.489	5.030	–	–	υ_{CC}(37) C
1641	1587	0.301	23.20	1592	–	υ_{CC}(39) δ_{CCC}(11) C
1643	1589	3.052	11.01	–	–	υ_{CC}(32) B
1652	1598	9.487	3.144	–	–	δ_{HNH}(30) + υ_{CC}(14)A
1667	1612	54.22	100	–	–	δ_{HNH}(50)
1696	1640	100	89.41	–	1603	υ_{OC}(75)
3165	3023	2.908	2.450	–	3069	υ_{CH}(93) A
3167	3024	0.115	0.073	–	–	υ_{CH}(96) C
3177	3034	1.733	1.431	–	–	υ_{CH}(97) C
3179	3036	1.932	0.784	–	3127	υ_{CH}(99) A

Table 3 (*continued*)

Unscaled frequency[a]	Scaled frequency[b]	I_{IR}[c]	I_{Raman}[d]	Exp. IR	Exp. Raman	TED[e] (%)
3187	3044	4.359	3.638	–	–	υ_{CH}(91) C
3196	3052	0.699	1.730	–	–	υ_{CH}(93) A
3196	3053	2.089	0.970	–	–	υ_{CH}(94) C
3208	3064	0.790	0.677	–	–	υ_{CH}(90) C
3222	3077	0.325	0.354	–	–	υ_{CH}(97) B
3572	3412	8.110	10.14	3344	3347	υ_{NH}(100)
3671	3505	4.285	4.404	3422	–	υ_{NH}(100)

P: phenyl (C ring), R: A and B rings, υ: stretching, δ: bending, Γ: torsion.
[a] Unscaled frequencies.
[b] Obtained from the wave numbers calculated at B3LYP/6-311++G(d,p) using scaling factors 0.967 (for wave numbers under 1800 cm^{-1}) and 0.955 (for those over 1800 cm^{-1}).
[c] Relative absorption intensities normalized with highest peak absorption equal to 100.
[d] Relative Raman intensities calculated by Eq. (1) and normalized to 100.
[e] Total energy distribution calculated B3LYP/6-311++G(d,p) level of theory. Only contributions $\geqslant$10% are listed.

The ring C–C stretching vibration occurs in the region 1625–1430 cm^{-1}. For six membered aromatic rings there are two or three bands in this region due to skeletal vibration the strongest usually being about 1500 cm^{-1}. In the case where the ring is conjugated further, a band about 1580 cm^{-1}. The C–C stretching of ring C is observed at 1592 cm^{-1} in IR. The same band is observed in IR at 1564 cm^{-1} and in Raman at 1565 cm^{-1} for the ring A. The aromatic ring deformation vibrations are appear in the region 625–605 cm^{-1} for the mono substituted ring and 475–425 cm^{-1} for the trisubstituted ring. The ring deformation of ring C is observed in IR at 599 cm^{-1} and in Raman at 616 cm^{-1}. The observed Raman band at 402 cm^{-1} is assigned for the ring deformation of the ring A.

4.5. HOMO–LUMO energy gap

In principle, there are several ways to calculate the excitation energies. The first, and the simplest one, involves the difference between the highest occupied molecular orbital (HOMO) and the lowest unoccupied molecular orbital (LUMO) of a neutral system. This form corresponds to the frozen orbital approximation, as the ground state properties are used to calculate excitation values. The HOMO–LUMO energy gap for 6AF has been calculated DFT level. The eigen values of LUMO and HOMO and their energy gap reflect the biological activity of the molecule. LUMO act as an electron donor which donates an electron. The atomic orbital compositions of the molecular orbitals are sketched in Fig. 6.

$$\text{HOMO energy} = -811.06\ \text{kJ mol}^{-1}$$

$$\text{LUMO energy} = -561.43\ \text{kJ mol}^{-1}$$

$$\text{HOMO—LUMO energy gap} = 249.63\ \text{kJ mol}^{-1}$$

The calculated self-consistent field (SCF) energy of 6AF is −2057434.002 kJ mol^{-1}. In addition, the decrease in the HOMO and LUMO energy gap explains the eventual charge transfer interaction taking place within the molecule which is responsible for the bioactivity of the molecule.

5. Conclusion

The detailed interpretation of the vibrational spectra has been carried out with the aid of normal coordinate analysis (NCA) following the scaled quantum mechanical force field methodology. FT-IR and FT-Raman spectra of the 6-aminoflavone have been recorded and analyzed. The molecular geometry, conformational stability, HOMO and LUMO energy, vibrational wavenumbers, of 6AF in the ground state has been calculated by using density functional theory. The optimized structure gives the non-planarity and π-electron delocalization of the structure. The observed and the calculated wavenumbers are found to be in good agreement. The lowering of carbonyl stretching wavenumber is due to the π-electron being localized. The lowering of the HOMO–LUMO energy gap value has substantial influence on the intramolecular charge transfer and bioactivity of the molecule.

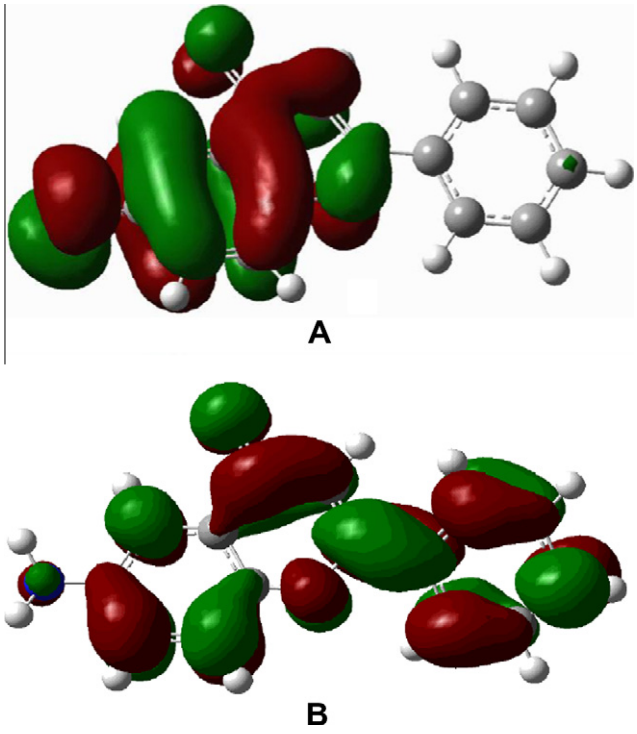

Fig. 6. HOMO (A) and LUMO (B) plot of 6AF.

Acknowledgement

This work was supported by the Research Fund of Ahi Evran University Project Number: A10/2009. We would like to thank the central laboratory of METU (ODTÜ) for recording FT-Raman spectra, Gazi University Art and Science Faculty Department of Chemistry for recording FT-IR spectra and Assoc. Prof. Dr. Mustafa KURT for Gaussian 03W program package.

References

[1] A.I. Loaiza-Pérez, S. Kenney, J. Boswell, M. Hollingshead, C. Hose, W.M. Linehan, R. Worrell, L. Rubinstein, E.A. Sausville, D.T. Vistica, J. Urol. 171 (2004) 1688–1697.
[2] M.J. Kuffel, J.C. Schroeder, L.J. Pobst, S. Naylor, J.M. Reid, S.H. Kaufmann, M.M. Ames, Mol. Pharmacol. 62 (2002) 143–153.

[3] T. Teslova, C. Corredor, R. Livingstone, T. Spataru, R.L. Birke, J.R. Lombardi, M.V. Canamares, M. Leona, J. Raman Spectrosc. 38 (2007) 802.
[4] J.B. Harborne, T.J. Marby, H. Marby, The Flavonoids, Chapman and Hall, London, 1975.
[5] J.B. Harborne, T.J. Marby, The Flavonoids: Advances in Research, Chapman and Hall, London, 1982.
[6] J.W. McClure, in: V. Cody, E. Middleton, J.B. Harborne (Eds.), Plant Flavonoids in Biology and Medicine: Biochemical, Pharmacological and Structure–Activity Relationships, Alan R. Liss, New York, 1986, p. 77.
[7] T.A. Geissman, The Chemistry of Flavonoid Compounds, The Macmillan Company, New York, 1962.
[8] D.A. Smith, S.W. Banks, in: V. Cody, E. Middleton, J.B. Harborne (Eds.), Plant Flavonoids in Biology and Medicine: Biochemical, Pharmacological and Structure–Activity Relationships, Alan R. Liss, NewYork, 1986, p. 113.
[9] M. Gabor, The Pharmacology of Benzopyrone Derivatives and Related Compounds, Budapest, Akademiai Kiado, 1986.
[10] H. Böhm, J. Boeing, J. Hempel, B. Raab, A. Kroke, Z. Ernährungswiss. 37 (1998) 147.
[11] K. Raghavan, J.K. Buolamwini, K.W. Kohn, J.N. Weinstein, J. Med. Chem. 38 (1995) 890.
[12] W.F. De Azevedo, H.J. Mueller-Dieckmann, U. Schulze Gahmen, P.J. Worland, E. Sausville, S.H. Kim, Proc. Natl. Acad. Sci. USA 93 (1996) 2735.
[13] L. Costantino, G. Rastelli, M.C. Gamberini, J.A. Vinson, P. Bose, A. Iannone, M. Staffieri, L. Antolini, A. Del Corso, U. Mura, A. Albasini, J. Med. Chem. 42 (1999) 1881.
[14] M.C. Etter, Z. Urbanczyk-Lipowska, S. Baer, P.F. Barbara, J. Mol. Struct. 144 (1986) 155.
[15] S. van Acker, A.B.E. de Groot, M.J. van den Berg, D.J. Tromp, G. Donne-Op den, M.N.L. Kelder, G. van der Vigh, W.J.F. Bast, Chem. Res. Toxicol. 9 (1996) 1305.
[16] J.P. Cornard, J.C. Merlin, A.C. Boudet, L. Vrielynk, Biospectroscopy 3 (1997) 183.
[17] J.P. Abraham, D. Sajan, J. Mathew, I.H. Joe, V. George, V.S. Jayakumar, J. Raman Spectrosc. 39 (2008) 1821.
[18] L. Vrielynck, J.P. Cornard, J.C. Merlin, M.F. Lautie, Spectrochim. Acta 50A (1993) 2177.
[19] G.K. Pereira, P.M. Donate, S.E. Galemeck, J. Mol. Struct. (Theochem) 363 (1996) 87.
[20] G.K. Pereira, P.M. Donate, S. Galemeck, J. Mol Struct (Theochem). 392 (1997) 169.
[21] H.M. Ishiki, P.M. Donate, S.E. Galemeck, J. Mol Struct (Theochem). 423 (1998) 235.
[22] M. Meyer, J. Quantum Chem. 76 (2000) 724.
[23] Y. Erdogdu, O. Unsalan, M.T. Gulluoglu, Turk. J. Phys. 33 (2009) 249.
[24] Y. Erdogdu, O. Unsalan, D. Sajan, M.T. Gulluoglu, Spectrochim. Acta A 76 (2010) 130–136.
[25] Y. Erdogdu, O. Unsalan, M.T. Gulluoglu, J. Raman Spectrosc. (2010), doi:10.1002/jrs.2520.
[26] O. Unsalan, Y. Erdogdu, M.T. Gulluoglu, J. Raman Spectrosc. 40 (5) (2009) 562.
[27] Gaussian 03, Revision C.02, M.J. Frisch, G.W. Trucks, H.B. Schlegel, G.E. Scuseria, M.A. Robb, J.R. Cheeseman, J.A. Montgomery, Jr., T. Vreven, K. N. Kudin, J.C. Burant, J.M. Millam, S.S. Iyengar, J. Tomasi, V. Barone, B. Mennucci, M. Cossi, G. Scalmani, N. Rega, G.A. Petersson, H. Nakatsuji, M. Hada, M. Ehara, K. Toyota, R. Fukuda, J. Hasegawa, M. Ishida, T. Nakajima, Y. Honda, O. Kitao, H. Nakai, M. Klene, X. Li, J.E. Knox, H.P. Hratchian, J.B. Cross, C. Adamo, J. Jaramillo, R. Gomperts, R.E. Stratmann, O. Yazyev, A.J. Austin, R. Cammi, C. Pomelli, J.W. Ochterski, P.Y. Ayala, K. Morokuma, G.A. Voth, P. Salvador, J.J. Dannenberg, V.G. Zakrzewski, S. Dapprich, A.D. Daniels, M.C. Strain, O. Farkas, D.K. Malick, A.D. Rabuck, K. Raghavachari, J.B. Foresman, J.V. Ortiz, Q. Cui, A.G. Baboul, S. Clifford, J. Cioslowski, B.B. Stefanov, G. Liu, A. Liashenko, P. Piskorz, I. Komaromi, R.L. Martin, D.J. Fox, T. Keith, M.A. Al-Laham, C.Y. Peng, A. Nanayakkara., M. Challacombe, P.M. W. Gill, B. Johnson, W. Chen, M.W. Wong, C. Gonzalez, and J.A. Pople, Gaussian, Inc., Wallingford CT, 2004.
[28] M.H. Jamróz, Vibrational Energy Distribution Analysis VEDA 4, Warsaw, 2004.
[29] A.E. Reed, L.A. Curtiss, F. Weinhold, Chem. Rev. 88 (1988) 899.
[30] J.P. Foster, F. Weinhold, J. Am. Chem. Soc. 102 (1980) 7211.
[31] F. Weinhold, C.R. Landis, Valency and Bonding: A Natural Bond Orbital Donor–Acceptor Perspective, Cambridge University Press, New York, 2005.
[32] H.W. Thomson, P. Torkington, J. Chem. Soc. (1945) 640.
[33] E.D. Glendening, J.K. Badenhoop, A.E. Reed, J.E. Carpenter, J.A. Bohmann, C.M. Morales, F. Weinhold, NBO 5.0, Theoretical Chemistry Institute, University of Wisconsin, Madison, 2001.
[34] J.N. Liu, Z.R. Chen, S.F. Yuan, J. Zhejiang Univ. Sci. B6 (2005) 584.
[35] C. James, A. Amal Raj, O.F. Nielson, V.S. Jayakumar, I. Hubert Joe, Spectrochim. Acta. 70A (2008) 1208.
[36] B. Smith, Infrared Spectral Interpretation: A Systematic Approach, CRC, Washington, DC, 1999.
[37] O. Alver, C. Parlak, Vib. Spectros. (2010), doi:10.1016/j.vibspec.2010.05.001.
[38] G. Keresztury, Raman spectroscopy: theory, in: J.M. Chalmers, P.R. Griffith (Eds.), Handbook of Vibrational Spectroscopy, vol. 1, John Wiley & Sons Ltd., New York, 2002, pp. 71–87.
[39] N. Puviarasan, V. Arjunan, S. Mohanan, Turk. J. Chem. 26 (2002) 323.
[40] H. Nakayama, M. Mukai, R. Hagiwara, K. Ishil, J. Phys. Chem. A 94 (1990) 4343.
[41] F.R. Dollish, W.G. Fateley, F.F. Bentley, Characteristic Raman Frequencies of Organic Compounds, Wiley, New York, 1974.